Mardali, M.; Salimijazi, H.; Karimzadeh, F.; Luthringer-Feyerabend, B.:
The effect of an MgO intermediate layer on a nanostructured HA coating fabricated by HVOF on an Mg alloy.
In: Surface and Coatings Technology. Vol. 374 (2019) 1071 - 1077.
First published online by Elsevier: 01.07.2019

https://dx.doi.org/10.1016/j.surfcoat.2019.06.092

The effect of an MgO intermediate layer on a nanostructured HA coating fabricated by HVOF on an Mg alloy

Marzieh Mardali[a, b], Hamidreza Salimijazi[a], Fathallah Karimzadeh[a], Berengere Luthringer-Feyerabend[b]

[a]Department of Materials Engineering, Isfahan University of Technology, Isfahan 84156-83111, Iran

[b]Institute of Materials Research, Helmholtz-Zentrum Geesthacht, 21502 Geesthacht, Germany

Abstract

Lightweight magnesium alloys are currently being investigated as implants due to their biodegradability and mechanical properties. However, their clinical applications are limited by their high corrosion rate in the physiological environment. Coating Mg-based alloys is an approach that is used to delay primary corrosion and increase their lifetime. Therefore, hydroxyapatite was coated on anodized and non-anodized magnesium substrates using high-velocity oxy-fuel spraying. This study aimed to evaluate the effect of the MgO intermediate layer between the hydroxyapatite coating and Mg alloy substrate. The microstructure and corrosion behaviour of the coated samples are the main focuses of this study. X-ray diffraction spectroscopy was used to analyse the phases. Electrochemical impedance spectroscopy was performed in simulated body fluid. The results revealed that the presence of an anodized layer increased corrosion resistance.

Keywords: High-velocity oxygen fuel, Anodizing, Magnesium, Corrosion rate

1. Introduction

Magnesium (Mg) alloys are promising materials due to their biodegradability in the physiological environment. Other advantages of these materials include decreased cost and inconvenience due to the avoidance of secondary surgeries after healing. Furthermore, Mg is a crucial element in the physiological environment, and its Young modulus is similar to that of bone, thus overcoming stress-shielding effects. However, it has some disadvantageous, such as a high corrosion rate, that prevent its clinical applications. A high corrosion rate leads to insufficient strength for bone healing. Another issue during corrosion is the release of hydrogen gas as a reaction product, which can damage forming tissues [1-5].

Several coating techniques, such as sol-gel [6], bio-mimetic coating [7], thermal spraying [8], electrochemical deposition [9], chemical vapor deposition (CVD), and physical vapor deposition (PVD) [10], have previously been applied to fabricate hydroxyapatite (HA) coatings to control the Mg corrosion rate. Among them, spraying technologies are widely used for coating implant surfaces with HA being the Plasma Spraying (PS) method in commercial use for implant prosthesis. Their wide renge application is due to their features, including easy process control and high efficiency for mass production. However, PS seems not to be suitable for depositing HA onto Mg substrates because of the heat generated in this technique and the relatively low melting point of magnesium. Abdullah C.W. Noorakma et al. used cold spray deposition to avoid such handicaps [11].

Compared with the plasma spraying technique, high-velocity oxy-fuel (HVOF) is a thermal spraying technique that uses a lower temperature and heat input. Therefore, it creates fewer phase transformations and amorphous phases in HA coatings [12-15].

Typically, an intermediate layer is often used to increase the adhesion of coatings to substrates and reduce the gradient of the thermal expansion coefficient between coatings and substrates.

However, studies on intermediate layers between HA coatings and magnesium substrates are limited. The main reason for using of the intermediate layers in the base of coatings for Mg alloys is enhanced corrosion performance [16].

Ji-Hoon Jo et al. used an MgF_2 interlayer as a protective layer for HA coating. According to their results on the immersion test in SBF, it was found that the Mg released ion content of the HA+ MgF2 double layer coating was much less than that of the single-layer HA coating [17]. Magnesium oxide coatings produced by electrochemical methods are among the most effective manners to control the high corrosion rate of magnesium-based alloys. Numerous studies have been performed to investigate the effect of these coatings on the corrosion resistance of magnesium-based alloy implants [18].

In recent years, investigators have attempted to use calcium phosphate compounds as additives in electrochemical coatings to enhance the bioactivity of implant surfaces by this composite coating. However, achieving a suitable percentage of stable-phase HA requires the control of the effective parameters in this process, which is difficult [19]. Here, the authors tried to coat an HA double layer on the anodized surface in order to increase bioactivity. In this case, phase controlling is much easier.

In previous studies, hydroxyapatite was coated on an anodized Mg-based alloy by HVOF and flame spraying [20, 21]. The effects of the magnesium oxide layer on the microstructure and electrochemistry were shown in this study.

2. Materials and methods

The substrate was composed of 5.50% Al, 1.5% Zn, 0.78% Mn, and <0.02% Si, and the remaining mass fraction was Mg. Specimens with sizes of 15×15×5 mm were degreased in NaOH (10 g in 100 ml water) at 70 °C for 5 min. The anodization treatment was carried out in 3 M KOH and 1.3 M $Na_3(PO_4)$ at 25 °C using a DC power supply (IPC-SL20200J, Iran) under a

constant voltage of 70 V for 60 min. The distance between two electrodes was 4 cm. The cathode consisted of a stainless steel plate (25×30×3 mm).

Characteristics of the initial synthesized HA powder have been previously described [20]. The particle size was in the range of 0.5-0.9 μm, and the particle morphology was semi-spherical. After spray drying, the size of agglomerates was 17-20.5 μm. To create the second layer, an HVOF torch spraying system (K2-GTV, Germany) was used for thermal spraying. The parameters for HVOF spraying included an 850 L/min oxygen flow rate, 24 L/h kerosene flow rate, 0.5 m/sec scan rate and 35 cm spray distance. These parameters were selected according to the parameters recommended by the device manufacturer. The HA coating delaminated from the substrate if the samples were coated with a thickness greater than 20 μm.

The phase composition of the coatings was analysed using X-ray diffraction (XRD) (Bruker, Germany). Line-scan elemental analysis of the cross-sectional microstructure of the samples was conducted by SEM (Bruker Nano GmbH, Germany) equipped with energy dispersive X-ray spectroscopy (EDX) instrumentation (Bruker, Germany). The crystallite size was obtained using the modified Scherrer formula (Eq. (1)) [22] as follows:

$$\ln \beta = \ln \frac{0.9\lambda}{D} + \ln \frac{1}{cos\theta}, \quad (1)$$

where β (rad) is the full-width half maximum of peaks (FWHM), θ (°) is the diffraction angle, λ (nm) is the wavelength of the X-ray (λ=0.154056 nm), and D (nm) is the grain size.

To obtain $\beta_{instrument}$, quartz (SiO_2) was used as a standard. Quantitative analysis of the phase composition was conducted using the Rietveld refinements method and structural models obtained from American Mineralogist Crystal Structure (AMS) Database reference files for the calcium phosphate, Mg and MgO phases. Maud software with the fundamental parameters approach was employed. Scale factor, specimen displacement, background as a fifth order

Chebyshev polynomial and 1/x function, crystallite size, micro-strain, and lattice parameters were refined parameters [23].

Profilometry analysis was carried out to evaluate the surface topography. In this measurement, images were acquired from a 14.5×14.5 mm surface and scanned.

Corrosion analysis of the coatings was performed by electrochemical impedance spectroscopy (EIS) in simulated body fluid (SBF) using a computer-controlled potentiostat system. SBF was prepared according to the composition suggested by Tang [24]. A setup with a working electrode (coated samples with an area of 0.5 cm^2), counter electrode (a spiral platinum wire) and reference electrode (saturated Ag/AgCl) was used. The frequency range was from 30 kHz to 0.1 Hz, and the AC signal amplitude was ±10 mV with RMS sinusoidal perturbations. The EIS spectra were analysed using Zview software (Scribner Associates Inc.). The measurements were repeated three times. The corroded surface of the samples was analysed using an optical microscope.

The samples were immersed in αMEM medium (Gibco™ 31966021, UK) for 5 days in an incubator (37 °C, 5% CO_2, and ca. 90% rH). To protect other sides of the sample from corrosion, they were masked with resin (methyl methacrylate). Changes in the pH and osmolality in the medium were monitored every day.

3. Results

The phase compositions of the anodized substrates and HA coatings with and without an anodized MgO layer, are shown in Fig 1. XRD patterns showed that the coatings were completely crystallized. The formation of the magnesium oxide phase on the anodized sample was verified. The majority of formed phases in the HA+ MgO sample consisted of HA (96.2%), but Mg (2.1%), α-TCP (tricalcium phosphate) (1.2%) and MgO (0.5%) were also observed. The calculated crystallite size of the HA phase in this sample was 36 nm. The HA-coated sample

contained HA (49%), Mg (43.8%), α-TCP (4.9%) and tetra calcium phosphate (3.2%) phases. The crystallite size of the HA phase in this sample was 38.6 nm.

Cross-sectional microstructures are shown in Fig 2. The HA-sprayed layer thickness of the HA coating (Fig 2a) was in the range of 5.7 to 10.5 μm. The HA-sprayed layer thickness of the HA+ MgO coating (Fig 2b) was between 2.1 and 11.8 μm. The MgO layer thickness in this sample was in the range of 1.8 to 2.5 μm. The homogeneity of the HA coating is shown in Fig 2c. The anodized layer thickness was in the range of 7.6 to 15.6 μm (Fig 2d). A decrease in the magnesium oxide layer thickness after the thermal spraying process indicated that this process had an abrasive effect on this layer.

The surface morphology of the samples is shown in Fig 3. Flattened splats, semi-melted particles and small amounts of un-melted particles were observed. During spraying, high-speed particles caused incomplete spreading of the splats, and the particles retained a spherical shape. The surface was rough as a result of the incomplete spreading and un-melted particles. For both morphologies, nanoscale surface roughness was observed.

Line-scan elemental analysis of the cross-sectional microstructures of the samples is shown in Fig 4. As shown in Fig 4a, the amount of Mg increased from left to right. This curve can be divided into the following two regions: the calcium phosphate layer and substrate layer. However, line-scan elemental analysis of the HA coating on the anodized substrate showed three areas, as shown in Fig 4b. From left to right, these areas include the HA coating, magnesium oxide layer and Mg substrate layer. Additionally, Fig 4c shows two regions of the magnesium oxide layer and the substrate layer for the anodized sample.

The mean roughness parameter (R_a) of the samples is shown in Fig 5. The mean roughness difference between the substrate and anodized surfaces was 2 μm, which was negligible. However, the roughness of the HA+MgO surface was less than that of the other surfaces. This

result indicated the HVOF coating reduced the roughness due to high-speed particles during the spraying process.

Fig 6 shows the EIS analysis results. Two capacitive loops were observed for all samples. The loop diameter of the HA + MgO coating was greater than that of the anodized coating. The EIS results analysed by Z-view software are shown in Table 1. The presence of the anodized layer affected the mass transfer impedance and charge transfer impedance. Fig 7 shows the surface of the samples after EIS. Pitting caused by magnesium corrosion was observed on the bare alloy surface and HA-coated surface. However, this effect was less prominent on the HA + MgO sample.

Well plates containing samples immersed in αMEM medium after 24 h of incubation are shown in Fig 8. Hydrogen gas bubbles in the well containing the bare alloy were more prominent than in the wells containing the other alloys. High-rate corrosion products of the magnesium-based alloy were also observed for the bare alloy. The intensity of bubbling for the HA + MgO-coated sample was the lowest, indicating a low corrosion rate.

Changes in the pH and osmolality are shown in Fig 9. The pH value of the HA + MgO coating initially increased and eventually decreased. Osmolality refers to as the number of molar ions in a solution. An increase in osmolality can be caused by an increased corrosion rate. The changes in osmolality were similar to changes in the pH variations.

4. Discussion

The presence of an anodized layer on a substrate affects the phases formed in HA coatings. The thermal conductivity of ceramics is less than that of metals [25]. Therefore, by anodizing the substrate surface, the cooling rate of HA particles sprayed on the substrate is reduced. It was expected that more stable phases form in the HA + MgO coating than when the thermal

conductivity of the substrate was greater in the HA coating. For this reason, the percentage of tricalcium phosphate in the HA + MgO coating was 1.2%. The tricalcium phosphate percentage in the HA coating was 4.9%, and the tetra-calcium phosphate phase in this sample was 3.2%. The HA coating without the anodizing treatment contained $Ca_4(PO_4)_2O$, while the coating with the anodizing treatment did not contain $Ca_4(PO_4)_2O$. This result indicated the effect of the substrate on the formed phases in the thermally sprayed coating. In the coating on the anodized layer, the sprayed calcium phosphate particles cooled more slowly and thus had more stable phases due to the lower heat transfer coefficient at the surface of substrate (CTE_{MgO}= 0.36 $Wm^{-1}K^{-1}$ [26] and CTE_{Mg}= 156 $Wm^{-1}K^{-1}$ [27]). Intermediate phases, such as tricalcium phosphate and tetra-calcium phosphate, are more soluble in SBF. Therefore, decreased corrosion resistance of coatings with more intermediate phases is expected.

For the cross-sectional microstructure of the coatings, the HA coating created by high-speed thermal spraying had some voids and empty spaces between the splats and micro-cracks. Therefore, this coating was not as effective as the anodized layer for the reduction of the Mg corrosion rate.

Different parameters, such as pore resistance and double-layer capacitance, have serial or parallel effects on the final impedance. A capacitive loop at high frequencies is related to the charge transfer reaction (R_{ct}). A capacitive loop at low frequencies is related to mass transfer processes in the solid phase (R_{pore}) [28]. Compared with other plots, the Bode plots showed that the increase in impedance for the HA + MgO coating at low frequencies indicated the high corrosion resistance of this coating.

The impedance of the HA coating was less than that of the anodized sample. Furthermore, the impedance of the HA + MgO coating was greater than that of the anodized coating, indicating that the HA coating created on the anodized substrate reduced the corrosion of the substrate. In

fact, the HA coating, which acted as a space barrier between the corrosive solution and substrate, caused a delay in corrosion (Table 1).

The osmolality and pH during immersion of the HA + MgO coating in αMEM medium first increased and then decreased due to the decreased corrosion rate. As shown in Fig 8a, in the final days, the pH of all solutions decreased, which could be due to the deposition of degradation products on the surface because the formation of these products consumed hydroxyl groups (OH^-). As shown in Fig 8b, precipitation of corrosion products, such as magnesium hydroxide compounds and calcium magnesium phosphate on the surface, caused magnesium ions in the solution to be consumed, which reduced magnesium ion content on the 4th and 5th days. In fact, the release of magnesium ions and their consumption by depositing degradation products led to a steady-state magnesium ion concentration over time. Notably, for the calcium phosphate-coated samples, not only magnesium ions but also calcium, phosphorus and hydroxyl ions contributed to the osmolality [29].

5. Conclusions

The thermally sprayed HA coating on the Mg alloy substrate increased corrosion resistance. However, the presence of cracks and the uniformity of this layer influenced this behaviour. Then, to increase this corrosion resistance, an intermediate layer of magnesium oxide was used. The presence of the MgO layer increased the amount of stable phases in the HA layer. By adding the intermediate layer, the amount of hydrogen generated by magnesium corrosion was reduced.

Acknowledgements

We acknowledge the financial support received from the Isfahan University of Technology of Iran and Helmholtz Zentrum Geesthacht of Germany.

References

1. C. Castellani, R. A. Lindtner, P. Hausbrandt, E. Tschegg, S. E. Stanzl-Tschegg, G.

Zanoni, S. Beck, A. M. Weinberg, Bone–implant interface strength and osseointegration: Biodegradable magnesium alloy versus standard titanium control, Acta Biomater. 7 (2011) 432–440.

2. B. Ben-Nissan, Advances in Calcium Phosphate Biomaterials, first ed., Springer, Berlin Heidelberg, 2014.
3. *G. L. Song,* Corrosion Prevention of Magnesium Alloys, first ed., Woodhead Publishing, 2013.
4. G. Eddy, J. Poinern, S. Brundavanam, D. Fawcett, Biomedical Magnesium Alloys: A Review of Material Properties, Surface Modifications and Potential as a Biodegradable Orthopaedic Implant, Am. J. Biomed. Eng. 2 (2013) 218–240.
5. S. Virtanen, Biodegradable Mg and Mg alloys: Corrosion and biocompatibility, Mater. Sci. Eng. B Solid-State Mater. Adv. Technol. 176 (2011) 1600–1608.
6. C. Domínguez-Trujillo, E. Peón, E. Chicardi, H. Pérez, J. A. Rodríguez-Ortiz, J. J. Pavón, J. García-Couce, J. C. Galván, F. García-Moreno, Y. Torres, Sol-gel deposition of hydroxyapatite coatings on porous titanium for biomedical applications, Surf. Coatings Technol. 333 (2018) 158–162.
7. M. R. Mucalo*,* Hydroxyapatite (HAp) for Biomedical Applications, Woodhead Publishing Series in Biomaterials, (2015), p 289–306.
8. S. A. Adeleke, S. Ramesh, A. R. Bushroa Y. C. Ching, I. Sopyan, M. A. Maleque, S. Krishnasamy, H. Chandran, H. Misran, U. Sutharsini, The properties of hydroxyapatite ceramic coatings produced by plasma electrolytic oxidation, Ceram. Int. 44 (2018) 1802–1811.
9. M. Mohedano, B. J. C. Luthringer, B. Mingo, F. Feyerabend, R. Arrabal, P. J. Sanchez-Egido, C. Blawert, R. Willumeit-Römer, M. L. Zheludkevich, E. Matykina, Bioactive plasma electrolytic oxidation coatings on Mg-Ca alloy to control degradation behaviour,

Surf. Coatings Technol. 315 (2017) 454–467.

10. H. Hornberger, S. Virtanen, A. R. Boccaccini, Biomedical coatings on magnesium alloys - A review, Acta Biomater. 8 (2012) 2442–2455.
11. A. W. Noorakma, H. Zuhailawati, V. Aishvarya, B. K. Dhindaw, Hydroxyapatite-coated magnesium-based biodegradable alloy: cold spray deposition and simulated body fluid studies. J Mater Eng Perform. 22 (2013) 2997–3004.
12. R. B. Heimann, H. D. Lehmann, Bioceramic Coatings for Medical Implants: Trends and Techniques, first ed., Wiley-VCH Verlag GmbH & Co, Weinheim, 2015.
13. J. D. Haman, A. A. Boulware, L. C. Lucas, D. E. Crawmer, High-velocity oxyfuel thermal spray coatings for biomedical applications, J. Therm. Spray Technol. 4 (1995) 179–184.
14. J. Fernández, M. Gaona, J. M. Guilemany, Effect of Heat Treatments on HVOF Hydroxyapatite Coatings, J. Therm. Spray Technol. 16 (2007) 220–228.
15. S. Hasan, J. Stokes, Design of experiment analysis of the Sulzer Metco DJ high velocity oxy-fuel coating of hydroxyapatite for orthopedic applications, J. Therm. Spray Technol. 20 (2011) 186–194.
16. G. L. Song, Z. Shi, Corrosion mechanism and evaluation of anodized magnesium alloys, Corros. Sci. 85 (2014) 126-140.
17. J. H. Jo, B. G. Kang, K. S. Shin, H. E. Kim, B. D. Hahn, D. S. Park, Y. H. Koh, Hydroxyapatite coating on magnesium with MgF_2 interlayer for enhanced corrosion resistance and biocompatibility, J Mater Sci: Mater Med. 22 (2011) 2437–2447.
18. T. Lei, C. Ouyang, W. Tang, L. F. Li, L. S. Zhou, Enhanced corrosion protection of MgO coatings on magnesium alloy deposited by an anodic electrodeposition process, Corros Sci. 52 (10) (2010) 3504-3508.

19. J. Yang, X. Lu, C. Blawert, S. Di, M. L. Zheludkevich, Microstructure and corrosion behavior of Ca/P coatings prepared on magnesium by plasma electrolytic oxidation, Surf Coat Tech. 319 (2017) 359–369.
20. M. Mardali, H. SalimiJazi, F. Karimzadeh, B. Luthringer, C. Blawert, S. Labbaf, Fabrication and characterization of nanostructured hydroxyapatite coating on Mg-based alloy by high-velocity oxygen fuel spraying, Ceram. Int. 44 (12) (2018) 14667-14676.
21. M. Mardali, H. SalimiJazi, F. Karimzadeh, B. Luthringer, C. Blawert, S. Labbaf, Comparative study on microstructure and corrosion behavior of nanostructured hydroxyapatite coatings deposited by high velocity oxygen fuel and flame spraying on AZ61 magnesium based substrates, Appl. Surf. Sci. 465 (28) (2019) 614-624.
22. H. Tang, D.Z. Yu, Y. Luo, F.P. Wang, Preparation and characterization of HA microflowers coating on AZ31 magnesium alloy by micro-arc oxidation and a solution treatment, Appl. Surf. Sci. 264 (2013) 816-822.
23. Y.-T. Chiang, D.P. Birnie III, W.D. Kingery, Physical Ceramics, first ed., Wiley, New York, 1997.
24. M. N. Linaha, O. C. Meludub, M. E. Kundwalc, Comparison of heat transfer properties of dry sand and magnesium oxide powder by single probe method, Jurnal Teknologi. 77 (13) (2015) 93–97.
25. S. Lee, H. J. Ham, S. Y. Kwon, S. W. Kim, C. M. Suh, Thermal Conductivity of Magnesium Alloys in the Temperature Range from −125 °C to 400 °C, Int J Thermophys. 34 (2013) 2343–2350.
26. M. Razavi, M. Fathi, O. Savabi, D. Vashaee, L. Tayebi, In vitro study of nanostructured diopside coating on Mg alloy orthopedic implants, *Mater Sci Eng C*. 41 (2014) 168-177.

27. Y. Song, S. Zhang, J. Li, C. Zhao, X. Zhang, Electrodeposition of Ca-P coatings on biodegradable Mg alloy: in vitro biomineralization behavior, Acta Biomater. 36 (2010) 6-42.

Table 1. Electrochemical corrosion parameters of the SA, SH and SHM samples obtained from electrochemical impedance spectroscopy (EIS)

	R_s (ohm)	R_{pore} (ohm)	R_{ct} (ohm)	CPE_{dl} (10^{-3} Fcm^{-2})	CPE_{ct} (10^{-6} Fcm^{-2})
Substrate	41.7±0.9	52.1±1.2	64.5±0.8	0.68±0.05	0.15±0.08
Anodized layer	41±1.4	156.3±1.4	196±3.3	0.98±0.6	0.4±0.12

HA coating + MgO	41.2±2	274±2.1	306.3±1.3	1.13±0.5	0.17±0.01
HA coating	42±0.5	152±4.2	180.2±2.5	0.65±0.1	0.25±0.06

Fig 1. XRD patterns of the formed phases in the anodized, HA+ MgO-coated and HA-coated samples.

Fig 2. Cross-sectional microstructure of the a) HA-coated, b) anodized smple, c) HA + MgO double-layer-coated, d) HA + MgO at a higher magnification.

Fig 3. Surface morphology of the a) HA and b) HA+MgO coatings; F = flattened splat; U = un-melted particle; S = semi-melted particle; and I= inter-splat microcrack.

Fig 4. Linear elemental analysis of the a) HA coating, b) HA + MgO and c) anodized layer cross-sections.

Fig 5. Average roughness of the samples.

Fig 6. a) Nyquist, b) Bode and c) equivalent circuit plots for modelling the EIS data.

Fig 6. Corroded surfaces of the a) bare alloy, b) HA coating and c) HA + MgO coating after electrochemical impedance spectroscopy in SBF.

Fig 7. Images of the a) bare alloy, b) HA coating and c) HA + MgO coating after 5 days of immersion in αMEM medium.

Fig 8. Changes in the A) pH and b) osmolality over the course of 5 days of immersion in αMEM medium.

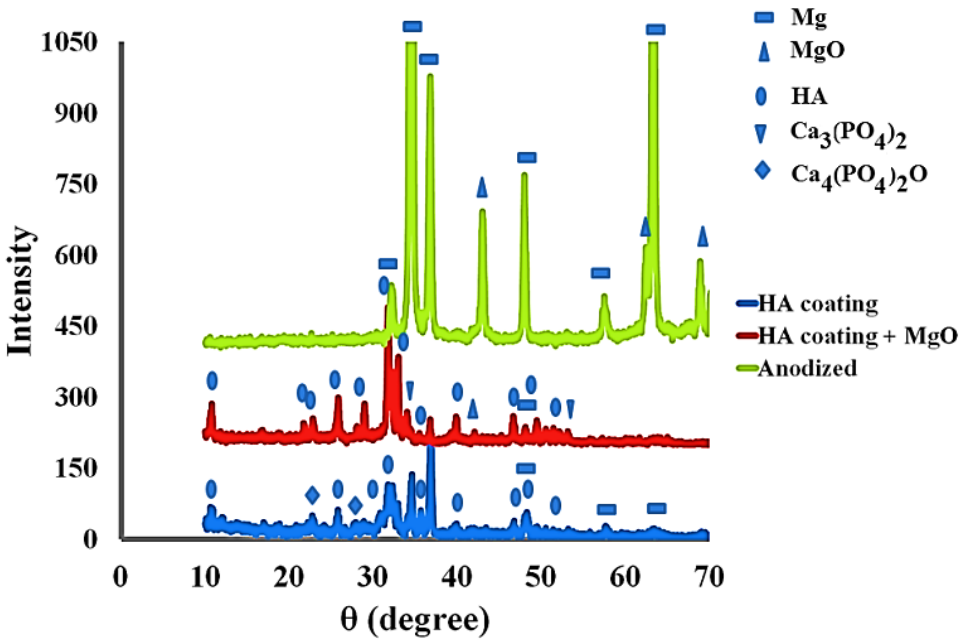
Mg
MgO
HA
Ca3(PO4)2
Ca4(PO4)2O
HA coating
HA coating + MgO
Anodized
Intensity
1050
900
750
600
450
300
150
0
0
10
20
30
40
50
60
70
θ (degree)

Fig 1

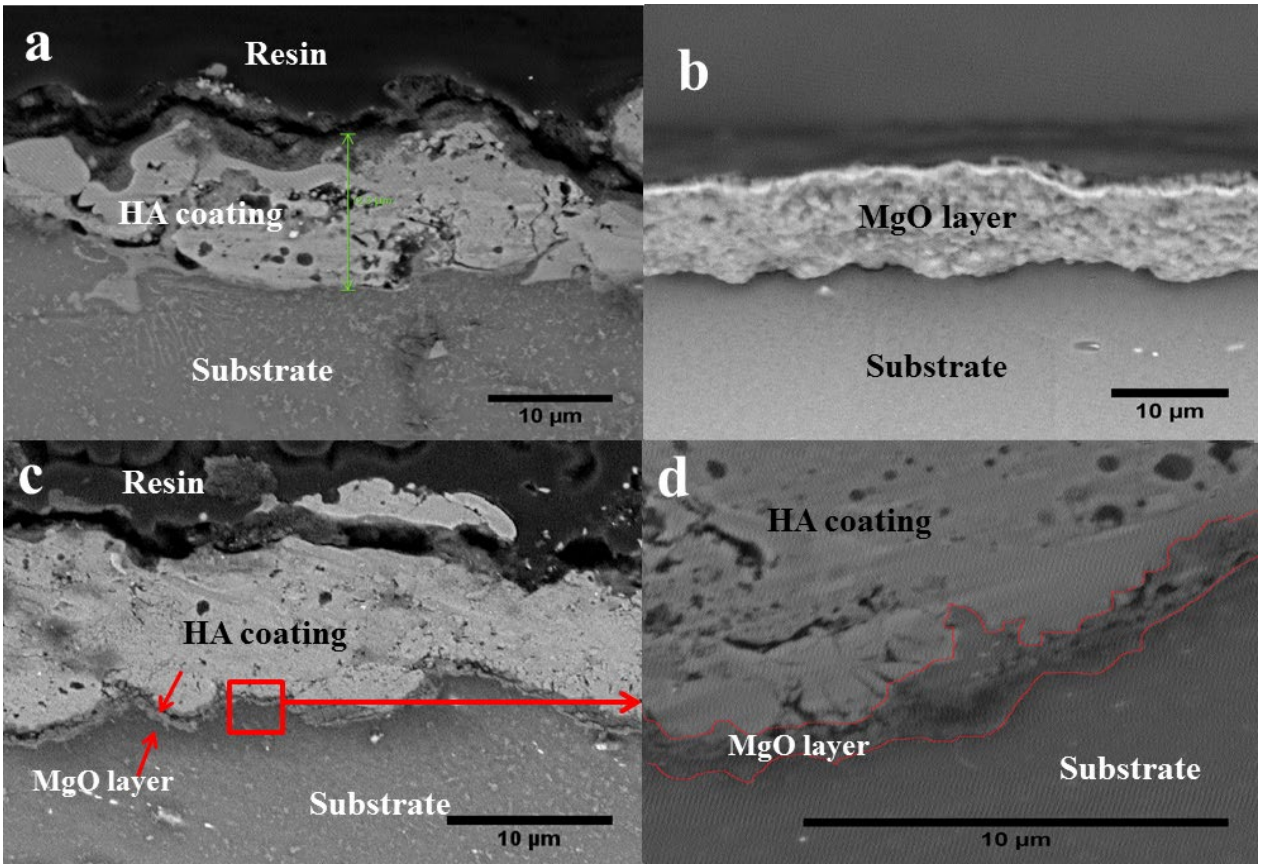
a
Resin
HA coating
Substrate
10 μm
b
MgO layer
Substrate
10 μm
c
Resin
HA coating
MgQ layer
Substrate
10 μm
d
HA coating
MgO layer
Substrate
10 μm

Fig 2

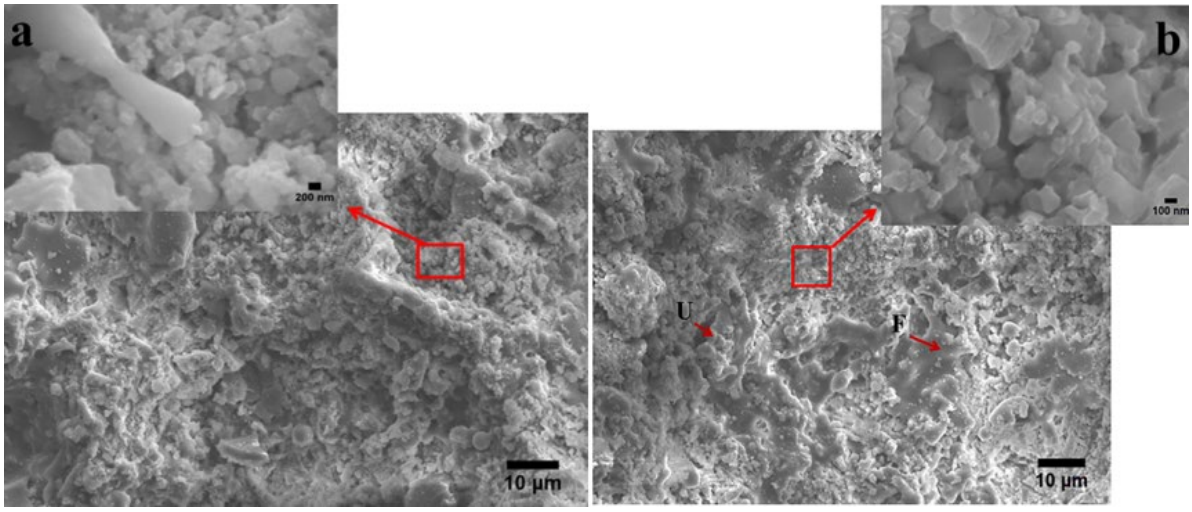

Fig 3

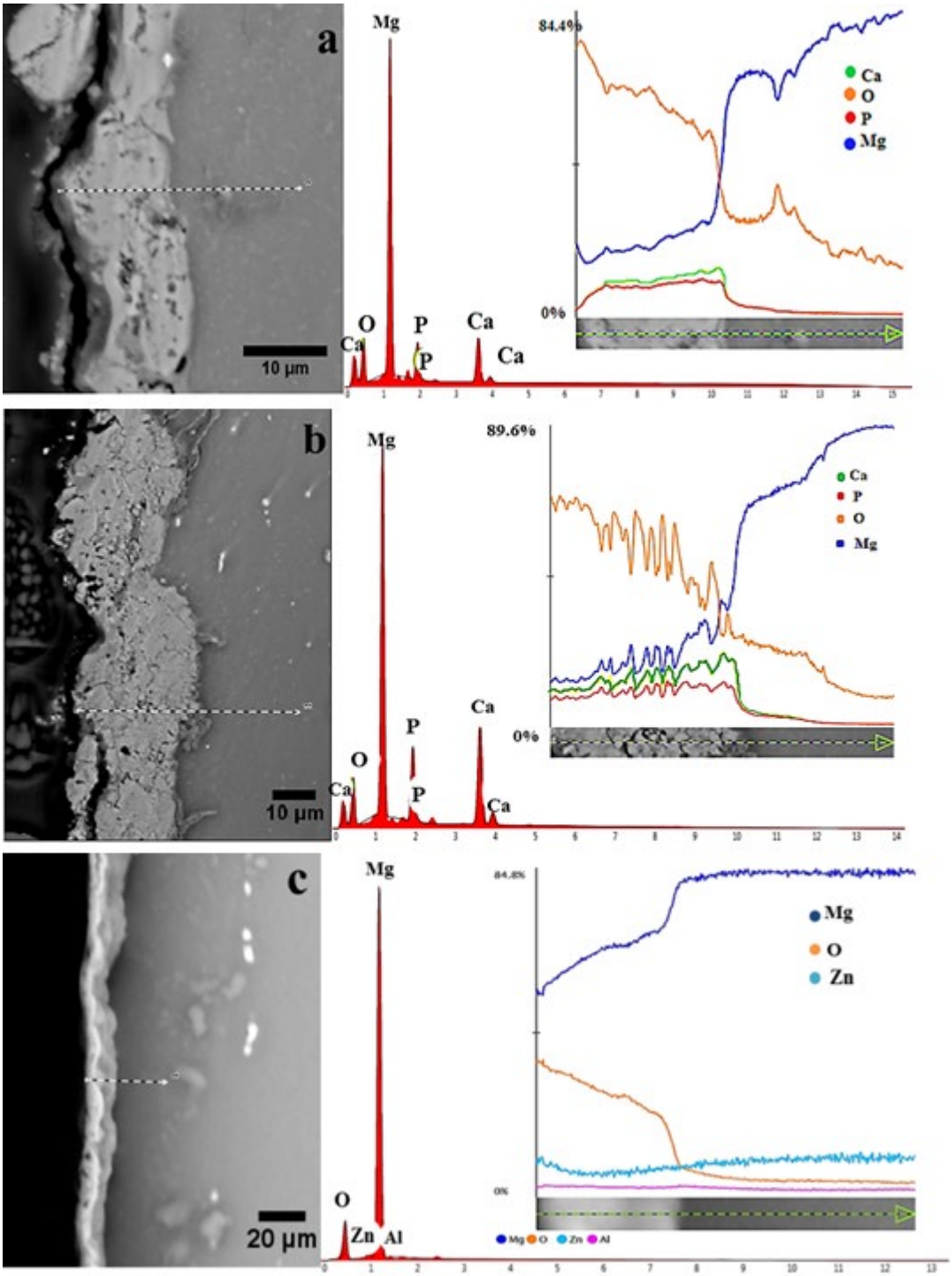
a
Mg
O
Ca
P
Ca
P
Ca
84.4%
Ca
O
P
Mg
0%
10 μm
b
Mg
O
Ca
P
P
Ca
Ca
89.6%
Ca
P
O
Mg
0%
10 μm
c
Mg
O
Zn
Al
84.8%
Mg
O
Zn
0%
20 μm

Fig 4

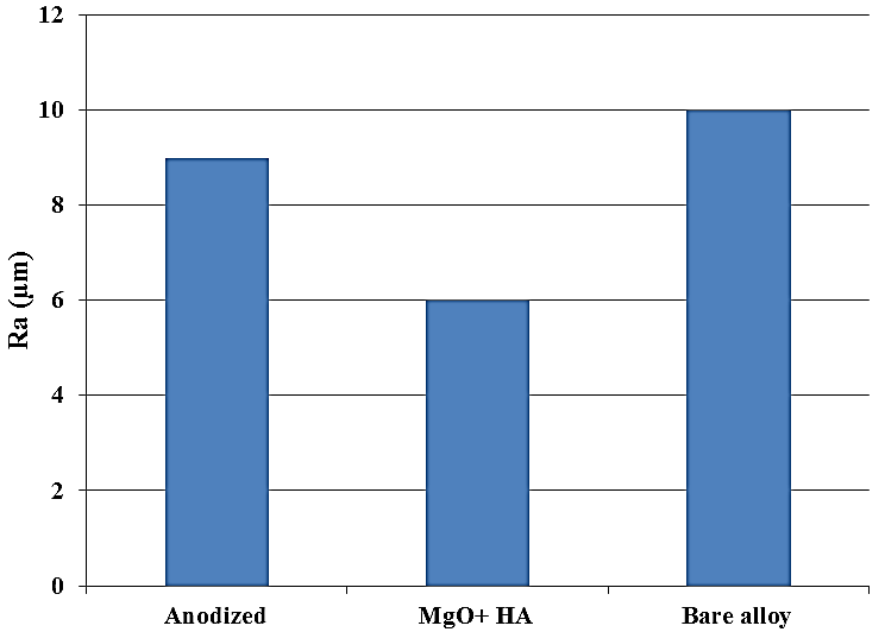
12
10
8
6
4
2
0
Ra (µm)
Anodized
MgO+ HA
Bare alloy

Fig 5

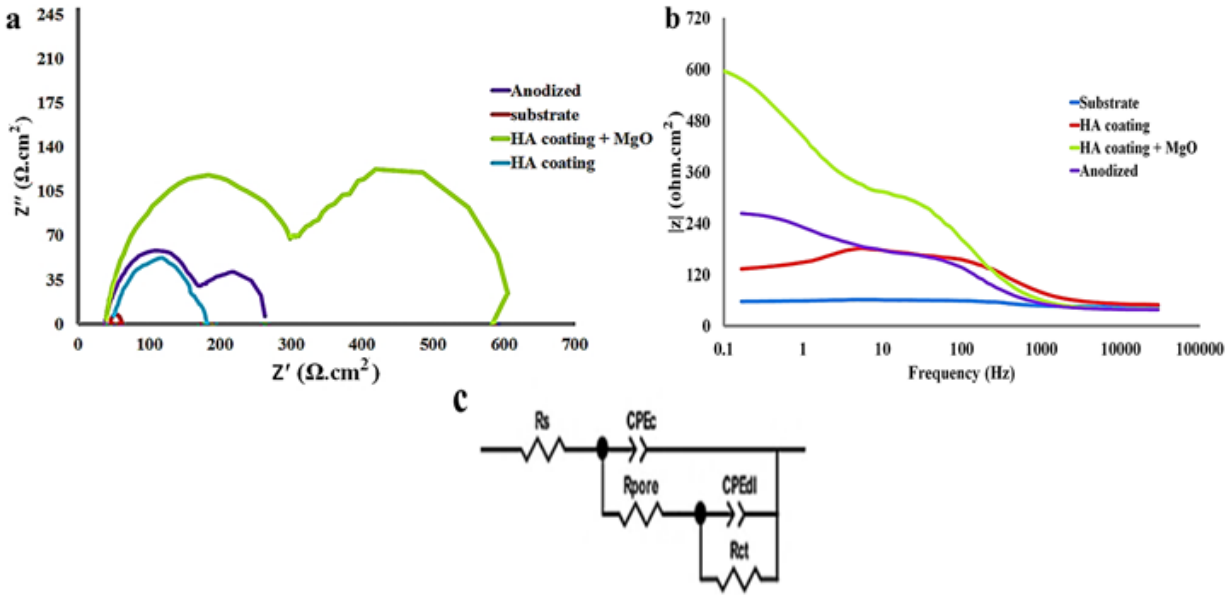
a
Z'' (Ω.cm²)
Z' (Ω.cm²)
Anodized
substrate
HA coating + MgO
HA coating
b
|Z| (ohm.cm²)
Frequency (Hz)
Substrate
HA coating
HA coating + MgO
Anodized
c
Rs
CPEc
Rpore
CPEdl
Rct

Fig 6

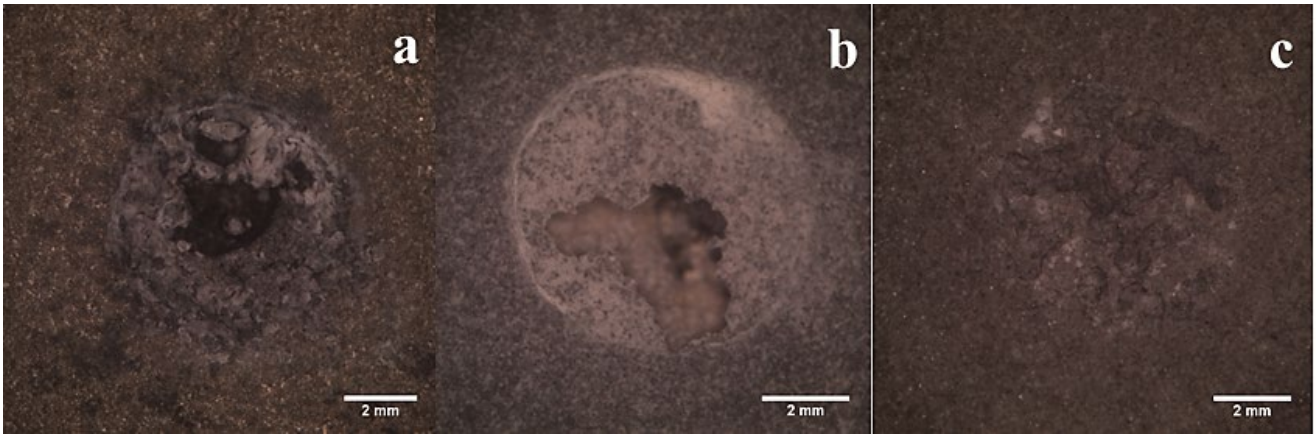

Fig 7

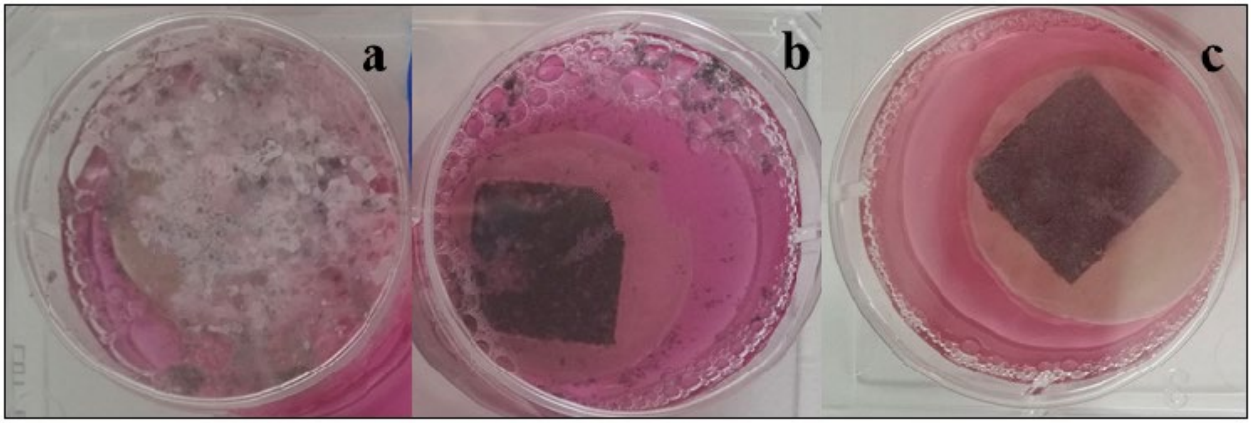

Fig 8

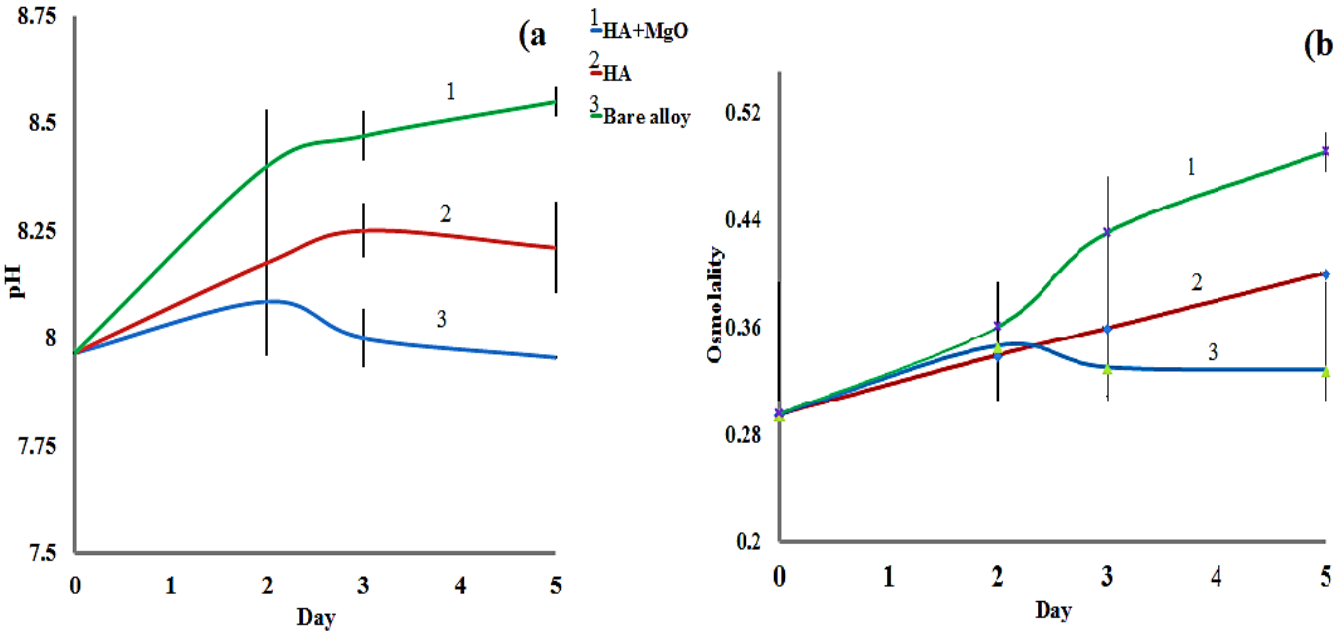
(a
1 HA+MgO
2 HA
3 Bare alloy
pH
8.75
8.5
8.25
8
7.75
7.5
0
1
2
3
4
5
Day
1
2
3
(b
Osmolality
0.52
0.44
0.36
0.28
0.2
0
1
2
3
4
5
Day
1
2
3

Fig 9